Energetics of Lanthanide-Doped Calcium Phosphate Apatite

Revision 1

S. Mahboobeh Hosseini[a,b], Christophe Drouet[c], Ahmed Al-Kattan[c], Alexandra Navrotsky[a,b]

[a] Peter A Rock Thermochemistry Laboratory and NEAT ORU, University of California Davis, One Shields Avenue, Davis, CA 95616

[b] Department of Chemical Engineering and Materials Science, University of California Davis, One Shields Avenue, Davis, CA 95616

[c] CIRIMAT Carnot Institute – Phosphates, Pharmacotechnics, Biomaterials Group, UMR CNRS/INPT/UPS 5085, University of Toulouse, 4 allée Emile Monso, 31030 Toulouse, France, christophe.drouet@ensiacet.fr

Corresponding author information:

Alexandra Navrotsky, *anavrotsky@ucdavis.edu*

Submitted to American Mineralogist

Revised May 11, 2014

Abstract

Lanthanides "Ln" (rare earths) are critical elements found in natural minerals such as calcium phosphate apatites, in sedimentary and igneous settings as well as in skeletal diagenesis. From a medical point of view, nanoparticles of lanthanide-doped apatites can be produced for conferring luminescence properties of interest in cancer cells detection. However, the impact of the substitution of Ln for Ca on the stability and solubility of related apatite phases is still essentially unknown. To investigate the thermochemical effects of such lanthanide substitution for calcium in apatite, we prepared and analyzed four series of apatites with up to 10 % lanthanide substitution for calcium. After thorough physicochemical characterization via complementary techniques (XRD, FTIR, TG/DSC and IPC-AES), high temperature oxide melt solution calorimetry in molten sodium molybdate at 973 K was performed to determine their enthalpies of formation from constituent oxides and from the elements, at 298 K. Our results indicate that although enthalpies of formation are strongly exothermic in all cases, Ln-doping has a destabilizing effect which increases with dopant concentration and with the size of the incorporated Ln^{3+} ion. After estimating standard entropies, Gibbs free energies of formation and equilibrium constants for Ca^{2+}/Ln^{3+} exchange reactions in apatite were then evaluated, for the first time allowing access to quantitative thermodynamic data that may be used in various fields for stability calculations or partitioning estimates between fluids and solids.

Keywords: calcium phosphate hydroxyapatite; lanthanide substitution; enthalpy of formation; calorimetry

Introduction

Apatites, corresponding to the general chemical formula $M_{10}(TO_4)_6X_2$, represent a large family of minerals commonly found in nature as both geological materials and biominerals in calcified tissues. In this versatile structure, M is often a divalent cation (e.g. Ca^{2+}, Sr^{2+}, and Pb^{2+}), TO_4 is an anionic group (e.g. PO_4^{3-}, SiO_4^{2-}, and VO_4^{3-}), and X is usually a monovalent anion (e.g. F^-, OH^-, and Cl^-), although ions exhibiting other valences (e.g. CO_3^{2-}, HPO_4^{2-}, O^{2-}, Na^+) may also be incorporated (Elliott, 1994).

Calcium phosphate hydroxyapatite ($Ca_{10}(PO_4)_6(OH)_2$), HA, is one of the most common apatite end-members. It is produced, with varying degrees of stoichiometry, by vertebrates for ensuring physico-chemical as well as mechanical functions of hard tissues (Gomez-Morales et al., 2013) and is also encountered in many other contexts including in the geochemistry, anthropology, and biomaterials fields (Anon, 2003; Bohner et al., 2008; Grunenwald et al., 2014; Prabakaran et al., 2005; Rabadjieva et al., 2010; Rodriguez-Lorenzo and Gross, 2003; Verron et al., 2010). Apatite with substantial fluorine substitution for hydroxyl (fluorapatite) occurs in both sedimentary and igneous settings, sometimes as massive deposits, which are mined as a source of phosphate for fertilizer, but which are also potential sources of the lanthanides (aka rare earths) which are considered critical elements for technology (Nagasawa, 1970; Reynard et al., 1999; Spear and Pyle, 2002). In the paleoanthropology domain, the analysis of skeletal remains has also pointed out the occurrence of lanthanides associated to the apatitic phase during bone/teeth diagenesis (Tutken et al., 2011; Kocsis et al., 1999; Trueman et al., 1999). The study of Ln incorporation in apatites can also help modeling the incorporation of radioactive actinide elements which are more complex to handle (Martin et al., 1999). Since it is compositionally and structurally close to the inorganic component of bones and teeth, hydroxyapatite is both biocompatible and bioactive, especially

in nanocrystalline and nonstoichiometric form (Drouet et al., 2005; Eichert et al., 2005; Elliott, 1994; Rey et al., 2007a; Rey et al., 2007b; Verron et al., 2010). Calcium phosphate apatite-based systems have therefore captivated the attention of biotechnology engineers for decades, and its use is now widespread in bone filling, prosthesis coating, and related applications (Cardoso et al., 2012; Rey et al., 2011). The last decades have produced numerous biomaterials based on apatite, sometimes associated with drugs or biologically active ions (Al-Kattan et al., 2010b; Barroug and Glimcher, 2002; Benaziz et al., 2001; Bohner et al., 2008; Drouet et al., 2008; Drouet et al., 2012; Iafisco et al., 2012; Weber et al., 2013). Biomimetic apatite-based hybrid systems have been used in cancer diagnosis and therapeutics (Al-Kattan et al., 2010a; Al-Kattan et al., 2011; Al-Kattan et al., 2010b; Al-Kattan et al., 2012; Bouladjine et al., 2009; Mondejar et al., 2007; Yang et al., 2008).

Despite this broad interest in apatites, structural and energetic studies relating to the incorporation of lanthanides into apatite remain infrequent. There remains a lack of understanding of the thermodynamics of formation of apatite compounds that may exhibit various degrees of stoichiometry, crystallinity, particle size, and ionic substitution. Published data almost invariably addresses only well-crystallized stoichiometric apatites (Jemal, 2011) (e.g. hydroxyapatite, fluorapatite, and apatites doped with heavy metals or alkaline earth ions), and the thermodynamic effects of lanthanide incorporation into phosphate apatites $M_{10}(PO_4)_6X_2$ do not seem to have been specifically addressed. In a recent study (Rollin-Martinet et al., 2013), we investigated by solution calorimetry the energetics of biomimetic apatites corresponding to various stoichiometries, documenting in particular their strongly negative enthalpy-driven Gibbs free energies of formation, and we related the formation energetics to changes in calcium and hydroxide contents, unveiling the importance of ionic substitution on apatite thermodynamics.

The aim of the current work is to explore the formation energetics of calcium phosphate hydroxyapatite obtained in wet conditions and doped by lanthanide (Ln^{3+}) ions, namely europium, erbium, neodymium, and terbium.

Experimental Methods

Sample synthesis and characterization

Ln-doped calcium phosphate hydroxyapatite samples (Ln = Eu, Er, Nd or Tb) were prepared by co-precipitation. Initial Ln/(Ln+Ca) molar ratios ranging between 0 and 0.10 (=10 %) were used. For each preparation, two starting solutions were prepared using deionized water. Solution A contained the proper amounts of $Ca(NO_3)_2{\cdot}4H_2O$ (Merck, Emsure) and $Ln(NO_3)_3{\cdot}nH_2O$ (Prolabo, analytical grade), and solution B contained the appropriate amount of $(NH_4)_2HPO_4$ (Prolabo, analytical grade). In a typical experiment, 12.5 ml of solution A (total initial Ca+Ln concentration: 0.4 M) was mixed with 12.5 ml of solution B (initial phosphate concentration: 0.13 M), at room temperature and under stirring for 30 min. The initial pH was set to 9.5 by addition of 20% ammonia (Fisher Scientific) under pH electrode control. The precipitate obtained after mixing was allowed to mature in an oven at 373 K for 16 h. The obtained suspension was then washed 6 times with deionized water using ultracentrifugation at 12,500 rpm to eliminate unreacted salts and undesired counter-ions. The purified suspensions were freeze-dried at 215 K for 3 days. The obtained powder samples are denoted "CaLnPx" where x represents the initial Ln/(Ca+Ln) molar ratio. For example, "CaEuP7" represents the sample precipitated in the presence of 7% of europium relative to the total Ca+Ln content.

$Eu(OH)_3$ was synthesized by precipitation in alkaline medium, using a mixture of europium nitrate and a few drops of concentrated NaOH (VWR, analytical grade). The europium nitrate was dissolved in deionized water and the solution was stirred for 5 min.

Then, NaOH was slowly added dropwise until precipitation, and the medium was heated at 90 °C overnight under constant stirring. The precipitate was centrifuged and washed 6 times with deionized water to remove residual ions. The final product was then oven-dried at 50 °C. This material was used for thermochemical measurements, as shown below.

Phase identification was carried out by powder X-ray diffraction (XRD) on a Bruker AXS D8 Advance diffractometer using Cu$K\alpha_1$ radiation (λ = 1.5406 Å), using a beam voltage of 40 kV and an emission current of 40 mA. A 0.02° step size from 10° to 90° 2θ with a 2 s/step dwell time was used as an acquisition parameter. MDI Jade software was used to identify the phases.

The presence of possible impurities, such as nitrate ions, was examined by Fourier transform infrared spectroscopy (FTIR) using KBr as a solid diluent, in the wavenumber range 400-4000 cm^{-1} (resolution 4 cm^{-1}), on a Nicolet 5700 spectrometer.

The Ca, P, Eu, Tb, Er, and Nd contents were measured at Marion Technologies S.A. (France) by inductively coupled plasma atomic emission spectroscopy, ICP-AES, with a relative uncertainty of 3%, using a Jobin Yvon apparatus (JY2000 model), after preliminary elemental calibrations (Chem-Lab reagents). Each measurement was performed starting from a volume of 50 ml of solution obtained by dissolving 10-15 mg of powdered sample in concentrated HCl, and followed by a 5-fold dilution. The following wavelengths were considered for the elemental titrations: 393.366 / 422.673 nm for Ca; 213.618 / 214.914 nm for P; 381.966 nm for Eu; 350.917 and 367.635 nm for Tb; 337.271 / 381.966 nm for Er and 406.109 / 430.357 nm for Nd. Tests were made in duplicate.

Differential scanning calorimetry (DSC) coupled with thermogravimetric analysis (TG) was performed on a Netzsch STA 449 at 25-1000 °C to measure the water content and follow potential phase transition/decomposition for each sample. About 25 mg of compound was

pelletized for each test. The sample was heated at 10 °C/min under synthetic air at a flow rate of 40 ml/min. Two runs were performed for each sample.

High temperature oxide melt solution calorimetry

Calorimetric experiments were carried out in a custom-built Tian-Calvet twin microcalorimeter. The equipment and experimental procedures have been described in detail by Navrotsky (Navrotsky, 1977; Navrotsky, 1997). Calibration of the calorimeter was based on the known heat content of ~ 5 mg α-Al_2O_3 pellets. The methodology was identical to that used in our recent study on biomimetic apatites (Rollin-Martinet et al., 2013).

Prior to drop solution calorimetry, the samples were hand-pressed into pellets (~ 5 mg), and weighed on a microbalance. The calorimetric experiments were performed by dropping the pellets, one by one, from room temperature (25 °C) into molten sodium molybdate solvent ($3Na_2O{\cdot}4MoO_3$) at 700 °C in the calorimeter. The measured heat effect, called the enthalpy of drop solution, ΔH_{ds}, is equal to the sum of the heat content of the sample, $\int_{298}^{700} C_{p,sample}\,dT$, and the heat of sample dissolution in sodium molybdate at 700 °C. During calorimetry, air was flushed through the calorimetric glassware assembly at 70 mL/min to expel any gases (e.g. water vapor) evolved in the calorimeter. Air was also bubbled through the solvent at 5 mL/min to facilitate the dissolution of the sample and thus avoid local solvent saturation. Complete dissolution of the sample in the solvent was verified during preliminary furnace experiments. At least 8 measurements were made for each sample. Two standard deviations of the mean are considered for evaluating the uncertainty of the data.

Results and Discussion

Sample characterization

The samples precipitated in the presence of lanthanide ions (Eu^{3+}, Er^{3+}, Nd^{3+}, or Tb^{3+}) with initial Ln/(Ln+Ca) molar ratios of 0, 0.01, 0.02, 0.04, 0.07 and 0.10 were first analyzed

by XRD for phase identification. In each case, the diffraction pattern showed the main characteristic peaks of an HA-like phase, thus confirming the formation of an apatitic compound. Typical XRD patterns obtained for the Eu series are shown in Figure 1, where the apatite phase has been indexed with respect to the JCPDS reference hydroxyapatite file # 09-432. Upon increasing the initial amount of lanthanide in the initial mixture, however, the presence of a secondary phase – identified as the corresponding lanthanide hydroxide $Ln(OH)_3$ – was also detected, and the relative proportions of apatite and lanthanide hydroxide were evaluated (see below).

The synthesis protocol used in this work was specifically selected because it is identical to the one used previously for the preparation of Ln-doped colloidal apatite nanoparticles (Al-Kattan et al., 2010a; Al-Kattan et al., 2014). Because it involves an excess of cations (Ca^{2+} + Ln^{3+}) over phosphate ions (relatively to the HA stoichiometry), as well as an alkaline pH, the formation of $Ln(OH)_3$ as a secondary phase for high Ln concentrations is not surprising. Limits to the amount of incorporated Ln^{3+} ions have indeed been shown (Al-Kattan et al., 2010a). Note that in the present study the presence of lanthanide phosphate $LnPO_4$ was never detected, which was also expected from our synthesis conditions (low phosphate content).

FTIR spectroscopy was used to characterize the precipitated samples. Very similar spectra were obtained for all samples. The vibrational data were found to support the XRD results in that the main vibration bands of a calcium phosphate apatite phase were detected in each sample. Figure 2 reports the typical case of Eu-doped samples. The presence of trace hydroxide ions in a secondary environment (i.e. within a $Ln(OH)_3$ lattice) was not detected by FTIR, which may be linked to the concomitant presence of hydration water molecules that give rise to a broad covering O-H vibration band around 3500 cm^{-1}.

Taking into account the XRD and FTIR findings, the prepared compounds are thus found to be composed of lanthanide-doped apatite associated to a secondary phase of lanthanide

hydroxide for high initial dopant amounts. Before further investigating the chemical composition of the samples, a question arises concerning the type of substitution mechanism for trivalent Ln^{3+} ions replacing divalent Ca^{2+} in the apatite lattice. Indeed, lanthanide incorporation can *a priori* occur by different substitution mechanisms. In the absence of monovalent cations (e.g. Na^{+}) or tetravalent anions (e.g. SiO_4^{4-}), four distinct substitution mechanisms can be envisioned (Al-Kattan et al., 2010a) for apatites obtained by wet chemistry (see Table 1).

If one hypothesizes that any of these four mechanisms, or a combination of them, is possible for the incorporation of trivalent lanthanide ions into the apatite structure, it should be possible to calculate the stoichiometry of each sample according to its Ln^{3+}/Ca^{2+} ratio and the specific substitution mechanism of interest. By applying the four model mechanisms independently to each sample, it appears that at low dopant concentrations ($y \leq 0.02$) all four mechanisms are possible. However, results from ICP-AES indicate that at high lanthanide concentrations, only mechanism 4 remains possible, since the other model mechanisms would result in negative values for the HPO_4^{2-} or OH^{-} contents. This mechanism implies, upon Ca-for-Ln substitution, the concomitant deprotonation of some OH^{-} ions, giving rise to O^{2-} anions in apatitic tunnels, which has already been reported in Ln-doped apatites (Taitai and Lacout, 1987; Ternane et al., 1999). In such scenarios, the high strength of the Eu-O bonds may be seen as a stabilizing factor (Piriou et al., 1987; Ternane et al., 1999). The existence of oxyapatite or oxyhydroxyapatite phases (for which a single O^{2-} takes the place of two OH^{-} in the apatite formula) is well-accepted (Yamashita et al., 1986), and could also hold at moderate to low temperatures, taking into account the Eu-O bond strength mentioned above. Despite the moderate temperature (100 °C) used for synthesis in the present study, we appear to observe mechanism 4, thus involving O^{2-} ions, at least for high Ln contents. Indeed, mechanism 4 is the only one to explain the experimental data for the whole series of samples

prepared in this work and will be considered to be the leading substitution scheme. For low Ln contents, other mechanisms (or a combination of mechanisms) listed in Table 1 may also come into play to some extent but they are not possible to determine here.

Once one major type of substitution mechanism is assumed, it becomes possible to define the chemical composition of the samples on the joint basis of ICP-AES, TG/DSC and XRD data. The numerical results obtained by considering mechanism 4 are reported in Table 2, per mole of doped apatite. In these calculations, as is customary for calcium phosphate apatites, the sum of the phosphates (PO_4^{3-} and HPO_4^{2-}) per mole of apatite was fixed at 6. This assumes complete occupation of the phosphate crystallographic sites due to the large size of the orthophosphate ion and the presumed structural instability that would arise from phosphate vacancies. Once a Ln/Ca substitution mechanism has been assumed (see Table 1), one has access to the chemical formula with two unknown parameters "x" and "y". In the case of mechanism 4, for instance, we have: $Ca_{10-x-y}Ln_y(PO_4)_{6-x}(HPO_4)_x(OH)_{2-x-y}(O)_y$. From ICP analyses, the Ln/(Ca+Ln) as well as the (Ca+Ln)/P ratios were measured. Then, having two equations with two unknown parameters, we could straightforwardly solve this mathematical system and find "x" and "y". This allowed the evaluation of the PO_4^{3-}/HPO_4^{2-} speciation as well as the OH^-/O^{2-} contents.

Based on Rietveld refinement of XRD data, the relative proportions of apatite and lanthanide hydroxide were concomitantly evaluated. TG/DSC measurements showed water loss (see also (Rollin-Martinet et al., 2013)) in the 25-212 °C range and the related weight loss permitted the evaluation of the amount of hydration water associated with the samples.

It may be noted (see final column of Table 2) that the experimental value of Ln/(Ca+Ln) in the apatite phase increases when the initial dopant concentration increases, although this trend levels out for the highest Ln concentrations. This tendency towards constancy of the experimental Ln content is indicative of the existence of a maximal substitution limit, as may

indeed be expected for such systems where trivalent cations replace divalent ones and where a second phase of $Ln(OH)_3$ defines the solubility limit.

As indicated in Table 2, an increased Ln^{3+} ion concentration in Ca-sites is accompanied by a decrease in the total amount of (O^{2-} + OH^-) and an increase of both HPO_4^{2-} and water content. Interestingly, a decrease in hydroxylation and an increase in HPO_4^{2-} were similarly observed for undoped nanocrystalline apatites of decreasing maturation states (Vandecandelaere et al., 2012). These findings suggest that lanthanide substitution decreases the overall degree of stoichiometry in the apatite phase. This suggests that Ln^{3+} ions play a role in apatite crystal growth inhibition, which is also the case of other ions such as Mg^{2+} or Zn^{2+} (Koutsoukos, 1998). Such inhibitory effects are complex phenomena, where the mode of interaction of the metal ion with the solid phase comes into play, as well as crystallographic considerations (especially when a trivalent ion replaces a divalent one as is the case for Ln^{3+}). Such a deviation from stoichiometry and decrease in degree of crystallinity are further confirmed in the present study on the basis of XRD data, where peak broadening was observed upon increasing Ln doping, thus pointing to a decrease in particle size which is in agreement with growth inhibition. This effect is, for example, visible on diffraction peak (002) (see inset in Figure 1). The estimation of crystallite dimensions is rather delicate as peak width is not only dependent on particle size, but also on the presence of microstrains which can be non-negligible for apatite compounds (Vandecandelaere et al., 2012). However, estimates of the mean crystallite length along the c-axis of the hexagonal unit cell have been tentatively calculated here using Scherrer's formula applied to the (002) peak, pointing out a decrease in mean crystallite length from *ca*. 40 nm down to about 25 nm when increasing the Ln content from 1 to 10%.

According to the XRD results, a single apatite phase was observed only for low dopant concentrations (typically less than y = 0.04). Beyond this limit, as mentioned above, $Ln(OH)_3$

formed as a secondary phase. However, the Ln incorporated amount continued to increase, thus indicating that the value of y = 0.04 may be an underestimation of the real solubility limit of the Ln^{3+} ions in the apatitic lattice in our synthesis conditions. The concomitant presence of apatite and $Ln(OH)_3$ phases may be related to not only thermodynamic but also kinetics aspects: the apatite phase being a complex oxide system with many ions to accommodate, its crystallization (especially if the incorporated ions act as growth inhibitors) requires time, allowing (at least in a transient way) secondary phases to be formed. In other words, our synthesis conditions do not allow complete equilibrium to be attained.

The composition of each sample, as listed in Table 2, was then taken into account in the energetic calculations below, so as to extract the enthalpy linked to the apatite phase alone.

Calorimetric measurements and thermodynamic properties of Ln-doped apatites

The experimental drop solution enthalpy (ΔH_{ds}) values for the calcium phosphate apatite samples prepared here are listed in Table 3, as well as values for the constituent binary oxides and lanthanide hydroxides $Ln(OH)_3$.

For samples containing a lanthanide hydroxide secondary phase (amount determined by XRD), the ΔH_{ds} of the apatite phase was determined by correcting the measured ΔH_{ds} for the two-component sample by the ΔH_{ds} of the lanthanide hydroxide phase alone. Therefore, the enthalpies of drop solution of the $Ln(OH)_3$ phases were also necessary to determine. As a starting point, the enthalpy of drop solution for $Eu(OH)_3$ was determined experimentally using a reference $Eu(OH)_3$ sample precipitated in this work (see experimental section). This experimental value of ΔH_{ds} for $Eu(OH)_3$ was then measured by drop solution calorimetry. Interestingly, this experimental value was found to be very close (within 2 kJ/mol, see Table 3) to the ΔH_{ds} value calculated using available thermodynamic data (i.e. using data for Eu_2O_3 and H_2O, see footnote "c" in Table 3). Considering this closeness between the calculated and

experimental values for $Eu(OH)_3$, and the potential difficulty to prepare pure $Ln(OH)_3$ phases, it was thus decided for the other lanthanide hydroxides to use enthalpies of drop solution (Table 3) calculated from values of the drop solution enthalpy of Ln_2O_3 and the formation enthalpy of $Ln(OH)_3$ from $Ln_2O_3 + H_2O$.

The enthalpies of formation of the apatitic phase alone (i.e. after removal of the $Ln(OH)_3$ contribution), from the constituent oxides at 25 °C ($\Delta H_{f,ox}$) using the thermodynamic cycle in Table 4, have been added to Table 3. Calculating enthalpies of formation from constituent binary oxides is particularly relevant as these values relate directly to the experimentally measured heats of drop solution, thus limiting the propagation of errors. The strongly exothermic values obtained for all studied systems indicate their significant stability with respect to the corresponding binary oxides. As discussed above, for low Ln^{3+} concentrations ($y \leq 0.02$), all four Ca^{2+}/Ln^{3+} substitution mechanisms theoretically remain possible. Accordingly, the calculated $\Delta H_{f,ox}$ values may somewhat fluctuate depending on the substitution mechanism, but we estimated this fluctuation to a maximum of 1.05 % around the values calculated here from mechanism 4. This confirms that enthalpy values calculated according to mechanism 4 are, from a practical viewpoint, fully relevant for evaluating the heats of formation of Ln-doped apatites. However, it also indicates that it is not possible here to determine the most favorable mechanism at low concentration from an energetic standpoint.

Figure 3 gives a graphical view of the variation, for each lanthanide ion, of $\Delta H_{f,ox}$ versus the experimental Ln/(Ca+Ln) molar ratio in the apatite. In each series, substituting lanthanide cations for calcium was found to significantly affect the energetics of the resulting apatite phase. The formation enthalpy becomes less exothermic upon increasing the dopant concentration. These findings point out the general tendency of Ln^{3+} incorporation to destabilize the (hydroxy)apatite system. These changes are likely due to charge and/or size

mismatch between the dopant (Ln^{3+}) and host (Ca^{2+}) cations and the corresponding charge balancing mechanism, here calculated as the creation of oxygen vacancies (mechanism 4). As shown in Figure 3, at low concentration of dopant, enthalpies of formation become less exothermic through an approximately linear relationship with dopant concentration. However, at higher concentrations, the enthalpies of formation tend to stabilize, indicating that we approach the solubility limit of incorporation of lanthanide in these systems.

To illustrate the effect of Ln^{3+} ionic size on energetics, the difference in formation enthalpies between doped and undoped systems was plotted against the dopant ionic radius, $r_{Ln^{3+}}$. Figure 4 reports the case of the experimental dopant concentration y = 0.04. This figure suggests that as the ionic radius of the dopant increases, the formation enthalpy tends to become less exothermic, indicating as a general tendency, a greater destabilizing effect for the larger lanthanide cations. However, this general trend is only approximate, taking into account the dispersion of the data points (e.g. Tb and Eu points are close to one another despite different radii). Thus ionic radius may not be the sole parameter in the variation of ΔH°_{f}, and other factors such as electronegativity or polarizability may play a role. Differences in maturation state, discussed further below, may also affect the energetics.

Enthalpies of formation $\Delta H^{\circ}_{f,el}$ (at 25 °C) from the elements in their standard states have also been calculated (Table 3). The value -13307.5 ± 12.4 kJ/mol obtained for the undoped apatite, which is slightly nonstoichiometric as compared to $Ca_{10}(PO_4)_6(OH)_2$, is slightly less exothermic than with the value measured previously for stoichiometric HA (-13431.0 ± 22.7 kJ/mol) (Rollin-Martinet et al., 2013). As expected, the general variation of $\Delta H^{\circ}_{f,el}$ for a given Ln^{3+} ion follows the same trend as evidenced above for $\Delta H^{\circ}_{f,ox}$, being less exothermic for increasing Ln^{3+} dopant content. Despite rather low amounts of incorporated Ln^{3+} cations, reaching about 10 % of the full cationic content, the destabilizing effect is quite significant, with a variation in enthalpy as compared to the undoped samples up to ca. 8 %. This

substantial destabilizing effect may possibly explain, at least in part, the low solubility limit of Ln^{3+} ions in the solid solution.

In the case of apatites, the relative stability can generally be assessed on the basis of enthalpy considerations, since the entropy contribution ($T\Delta S_f°$) in Gibbs free energies of formation ($\Delta G_f°$) remains low for such systems (Rollin-Martinet et al., 2013). However, it is interesting to evaluate the Gibbs free energies of formation $\Delta G_f°$ of these apatite compounds, which represent the "actual" stability parameters to take into account in thermodynamic calculations. To that aim, it was first necessary to estimate standard entropies S°. First approximations of S° were calculated by considering equilibrium reactions involving only solid phases (namely in this case calcium and lanthanide oxides or hydroxides), such as:

$$(9 - x - y/2)\ CaO\ (s, 298K) + (y/2)\ Ln_2O_3\ (s, 298K) + 3P_2O_5\ (s, 298K) + (1 - y/2)\ Ca(OH)2\ (s, 298K) \rightarrow Ca_{10-x-y}Ln_y(PO_4)_{6-x}(HPO_4)_x(OH)_{2-x-y}O_y$$

Eq. 1

Based on entropy values tabulated in thermodynamic databases for these oxide/hydroxide species and for the elements in their standard states, it was then possible to evaluate the S°, $\Delta S_f°$ and then $\Delta G_f°$ for the apatite samples prepared in this work. The values are reported in Table 5. As expected, $\Delta G_f°$ is again found to be mostly enthalpy-driven, with only a rather minor contribution of entropy.

Implications of Ln-Doping on the Stability of Apatite Compounds

Based on such evaluations of $\Delta G_f°$, it now becomes possible to investigate the effect of Ln doping on the stability of apatite and to estimate, for example, equilibrium constants for dissolution and partitioning reactions involving aqueous media.

Our characterization results (see above) clearly indicated that $Ln^{3+} = Eu^{3+}$, Er^{3+}, Nd^{3+}, and Tb^{3+} ions acted as apatite growth inhibitors. Therefore, Ln-doped apatites obtained via a given

set of experimental conditions will necessarily be less mature (i.e. exhibiting in particular a composition farther from stoichiometry) than apatites obtained in similar conditions but in the absence of Ln^{3+} ions in the medium. In this context, the comparison of doped and undoped samples becomes more delicate, as the maturation state of both the doped and undoped sample has to be taken into account.

The incorporation during synthesis of Ln^{3+} ions into the apatite lattice does not "simply" have a substituting role, it also influences the final structure and particle size state reached. Two phenomena have to be distinguished: a) the ionic substitution itself and b) the lower maturity of the apatite phase containing Ln.. If one considers (when comparing doped and undoped apatites) a common degree of maturity, then the two phenomena a) and b) might be separable.. But this remains a hypothetical situation. In real conditions, when the precipitation takes place in the presence of Ln^{3+} ions, the final apatite obtained exhibits a lower crystallinity state, higher nonstoichiometry, smaller particle size, and poorer crystallinity. . Consequently, if one intends to evaluate exclusively the energetic effect due solely to the incorporation in apatite of Ln^{3+} ions, the initial apatite system to consider in the reaction scheme (as illustrated in Equation 2 for mechanism 4) should be a phase with *equivalent* maturation state: This is very difficult to attain.

$$Ca_{10-x}(PO_4)_{6-x}(HPO_4)_x(OH)_{2-x} + y\ Ln^{3+}_{(aq)} + y\ OH^-_{(aq)} \leftrightarrow$$
$$Ca_{10-x-y}Ln_y(PO_4)_{6-x}(HPO_4)_x(OH)_{2-x-y}O_y + y\ Ca^{2+}_{(aq)} + y\ H_2O_{(liq)} \qquad \text{(Eq. 2)}$$

With the view to evaluate the variation in free energy accompanying Equation 2 ($\Delta G_{react} = \Delta G°_{react} + RTLn(K_{eq})$), it is thus not possible to use as initial apatite state the undoped compound prepared in this work (which exhibits a more advanced maturation stage). On the other hand, we have recently published data relative to the energetics of calcium phosphate apatites with various degrees of maturation (Rollin-Martinet et al., 2013). This

allowed us to evaluate $\Delta G°_{react}$ and K_{eq} (equilibrium constant at 25 °C) for systems presenting similar maturation patterns. For experimental Ln doping rates between 5 and 9 %, $\Delta G°_{react}$ values (not counting numbers lower than their propagated errors) were found between -62 ±18 and -377 ± 19 kJ/mol; and the corresponding values of pK_{eq} were found between -11 ± 7 and -66 ± 8. No clear ranking tendency was detectable in terms of $\Delta G_f°$ or K_{eq} values so as to distinguish the behavior of the four lanthanides studied in this work. However, these negative values point to a situation where Ln^{3+} incorporation (at least for the four lanthanides considered here) is energetically favorable – considering a constant maturation state – meaning that Equation 2 has a spontaneous tendency to evolve from left to right. It may be remarked that Equation 2 unveils a pH dependency through the involvement of OH^- ions. Considering ideal solid phases and water solvent (activities equal to unity), the equilibrium constant K_{eq} can thus be expressed as a function of ionic activities (shown by parentheses) as follows:

$$pK_{eq} = -y.Log\frac{(Ca^{2+})}{(Ln^{3+})} + y.(pH - 14) \qquad \text{Eq. 3}$$

Considering, as an illustrative example, a pH value of 9 and y = 0.5, Equation 3 would lead at 25 °C to a $(Ca^{2+})/(Ln^{3+})$ ratio typically ranging between 17 ± 10 and 127 ± 11, indicating a Ca^{2+} activity that is 1 or 2 orders of magnitude greater than that of Ln^{3+}.

Therefore, this work has shown, on a quantitative basis for the first time, that lanthanide ions (Ln^{3+}) can be accommodated in apatite with only small energetic destabilization of the solid phase. The thermochemical data reported in this work can be used to calculate the partitioning of Ln between apatite, fluids, melts, and other minerals. Such understanding of Ln distributions is relevant to a variety of fields including petrology, geochemistry, Ln mining

and processing, Ln transport in the environment, nanomedicine (use of Ln as phosphors in apatite in medical diagnostics) or else anthropology (diagenesis of skeletal remains).

Acknowledgments

This work was supported by the International Center of Materials Research (ICMR), the National Polytechnical Institute of Toulouse (INPT) and the France-Berkeley Fund (2008 call).

References

Al-Kattan, A., Dufour, P., Dexpert-Ghys, J., and Drouet, C. (2010a) Preparation and physicochemical characteristics of luminescent apatite-based colloids. Journal of Physical Chemistry C, 114(7), 2918-2924.

Al-Kattan, A., Dufour, P., and Drouet, C. (2011) Purification of biomimetic apatite-based hybrid colloids intended for biomedical applications: A dialysis study. Colloids and Surface B-Biointerfaces, 82(2), 378-384.

Al-Kattan, A., Errassifi, F., Sautereau, A., Sarda, S., Dufour, P., Barroug, A., Dos Santos, I., Combes, C., Grossin, D., Rey, C., and Drouet, C. (2010b) Medical potentialities of biomimetic apatites through adsorption, ionic substitution, and mineral/organic associations: Three illustrative examples. Advanced Engineering Materials, 12(7), B224-B233.

Al-Kattan, A., Girod-Fullana, S., Charvillat, C., Ternet-Fontebasso, H., Dufour, P., Dexpert-Ghys, J., Santran, V., Bordere, J., Pipy, B., Bernad, J., and Drouet, C. (2012) Biomimetic nanocrystalline apatites: Emerging perspectives in cancer diagnosis and treatment. International Journal of Pharmaceutics, 423(1), 26-36.

Al-Kattan, A., Santran, V., Dufour, P., Dexpert-Ghys, J., and Drouet, C. (2014) Novel contributions on luminescent apatite-based colloids intended for medical imaging. Journal of Biomaterials Applications, 28(5), 697-707.

Anon. (2003) Phosphates: Geochemical, geobiological, and materials importance. Reviews in Mineralogy and Geochemistry, volume 48. Matthew J. Kohn, John Rakovan, and John Hughes, eds. 1053-1054 p.

Barroug, A., and Glimcher, M.J. (2002) Hydroxyapatite crystals as a local delivery system for cisplatin: adsorption and release of cisplatin in vitro. Journal of Orthopaedic Research, 20(2), 274-280.

Benaziz, L., Barroug, A., Legrouri, A., Rey, C., and Lebugle, A. (2001) Adsorption of O-phospho-L-serine and L-serine onto poorly crystalline apatite. Journal of Colloid and Interface Science, 238(1), 48-53.

Bohner, M., Brunner, T.J., and Stark, W.J. (2008) Controlling the reactivity of calcium phosphate cements. Journal of Materials Chemistry, 18(46), 5669-5675.

Bouladjine, A., Al-Kattan, A., Dufour, P., and Drouet, C. (2009) New advances in nanocrystalline apatite colloids intended for cellular drug delivery. Langmuir, 25(20), 12256-12265.

Cardoso, D.A., Jansen, J.A., and Leeuwenburgh, S.C.G. (2012) Synthesis and application of nanostructured calcium phosphate ceramics for bone regeneration. Journal of Biomedical Materials Research Part B-Applied Biomaterials, 100B(8), 2316-2326.

Drouet, C., Carayon, M.-T., Combes, C., and Rey, C. (2005) Exchange of biologically relevant ions on nanocrystalline apatites. Geochimica et Cosmochimica Acta, 69(10), A69-A69.

-. (2008) Surface enrichment of biomimetic apatites with biologically-active ions Mg^{2+} and Sr^{2+}: A preamble to the activation of bone repair materials. Materials Science and Engineering C, 28(8), 1544-1550.

Drouet, C., Gomez-Morales, J., Iafisco, M., and Sarda, S. (2012) Calcium phosphate surface tailoring technologies for drug delivering and tissue engineering. In Surface Tailoring of Inorganic Materials for Biomedical Applications L. Rimondini, C.L. Bianchi, E. Vernè, Eds., p. 43-111. Bentham Science, e-book.

Eichert, D., Combes, C., Drouet, C., and Rey, C. (2005) Formation and evolution of hydrated surface layers of apatites. Bioceramics 17, 17, 3-6.

Elliott, J.C. (1994) Structure and Chemistry of the Apatites and Other Calcium Orthophosphates. Elsevier Science, Amsterdam.

Gomez-Morales, J., Iafisco, M., Manuel Delgado-Lopez, J., Sarda, S., and Drouet, C. (2013) Progress on the preparation of nanocrystalline apatites and surface characterization: Overview of fundamental and applied aspects. Progress in Crystal Growth and Characterization of Materials, 59(1), 1-46.

Grunenwald, A., Keyser, C., Sautereau, A.M., Crubezy, E., Ludes, B., and Drouet, C. (2014) Adsorption of DNA on biomimetic apatites: Toward the understanding of the role of bone and tooth mineral on the preservation of ancient DNA. Applied Surface Science, 292, 867-875.

Iafisco, M., Varoni, E., Di Foggia, M., Pietronave, S., Fini, M., Roveri, N., Rimondini, L., and Prat, M. (2012) Conjugation of hydroxyapatite nanocrystals with human immunoglobulin G for nanomedical applications. Colloids and Surfaces B-Biointerfaces, 90, 1-7.

Jemal, M. (2011) Thermochemistry and kinetics of the reactions of apatite phosphates with acid solutions. In Application of Thermodynamics to Biological and Materials Science, M. Tadashi, Ed. p. 547-572. InTech.

Kocsis, L. ,Trueman, C. N., Palmer, M. R. (2010) Protracted diagenetic alteration of REE contents in fossil bioapatites: Direct evidence from Lu-Hf isotope systematics. Geochimica Et Cosmochimica Acta, 74(21), 6077-6092.

Koutsoukos, P.G. (1998) Influence of metal ions on crystal growth of calcium phosphates. In Calcium Phosphates in Biological and Industrial Systems, p. 145-171. Kluwer Academic Publishers, Boston, Dordrecht, London.

Martin, P., Carlot, G., Chevarier, A., Den-Auwer, C., Panczer, G. (1999) Mechanisms involved in thermal diffusion of rare earth elements in apatite. Journal of Nuclear Materials, 275(3), 268-276.

Mondejar, S.P., Kovtun, A., and Epple, M. (2007) Lanthanide-doped calcium phosphate nanoparticles with high internal crystallinity and with a shell of DNA as fluorescent probes in cell experiments. Journal of Materials Chemistry, 17(39), 4153-4159.

Nagasawa, H. (1970) Rare earth concentrations in zircons and apatites and their host dacites and granites. Earth and Planetary Science Letters, 9(4), 359-364.

Navrotsky, A. (1977) Progress and new directions in high temperature calorimetry. Physics and Chemistry of Minerals, 2(1-2), 89-104.

-. (1997) Progress and new directions in high temperature calorimetry revisited. Physics and Chemistry of Minerals, 24(3), 222-241.

Piriou, B., Fahmi, D., Dexpertghys, J., Taitai, A., and Lacout, J.L. (1987) Unusual fluorescent properties of $Eu-^{3+}$ in oxyapatites. Journal of Luminescence, 39(2), 97-103.

Prabakaran, K., Balamurugan, A., and Rajeswari, S. (2005) Development of calcium phosphate based apatite from hen's eggshell. Bulletin of Materials Science, 28(2), 115-119.

Rabadjieva, D., Gergulova, R., Titorenkova, R., Tepavitcharova, S., Dyulgerova, E., Balarew, C., and Petrov, O. (2010) Biomimetic transformations of amorphous calcium phosphate: Kinetic and thermodynamic studies. Journal of Materials Science: Materials in Medicine, 21(9), 2501-2509.

Rey, C., Combes, C., Christophe, D., and Grossin, d. (2011) Bioactive Ceramics: Physical Chemistry. In Comprehensive Biomaterials, P. Ducheyne, K.E. Healy, D.W. Hutmacher, D.W. Grainger, and C.J. Kirkpatrick, Eds., 1, p. 187-221. Elsevier.

Rey, C., Combes, C., Drouet, C., Lebugle, A., Sfihi, H., and Barroug, A. (2007a) Nanocrystalline apatites in biological systems: Characterisation, structure and properties. Materialwissenschaft und Werkstofftechnik, 38(12), 996-1002.

Rey, C., Combes, C., Drouet, C., Sfihi, H., and Barroug, A. (2007b) Physico-chemical properties of nanocrystalline apatites: Implications for biominerals and biomaterials. Materials Science and Engineering C, 27(2), 198-205.

Reynard, B., Lecuyer, C., and Grandjean, P. (1999) Crystal-chemical controls on rare-earth element concentrations in fossil biogenic apatites and implications for paleoenvironmental reconstructions. Chemical Geology, 155(3-4), 233-241.

Robie, R.A., Hemingway, B.S., and Fisher, J.R. (1978) Thermodynamic properties of minerals and related substances at 298.15 K and 1 Bar (105 Pascals) pressure and at higher temperatures. United States Geological Survey Bulletin 1452, United States Government Printing Office, Washington, 456 pp p.

Rodriguez-Lorenzo, L.M., and Gross, K.A. (2003) Encapsulation of apatite particles for improvement in bone regeneration. Journal of Materials Science: Materials in Medicine, 14(11), 939-943.

Rollin-Martinet, S., Navrotsky, A., Champion, E., Grossin, D., and Drouet, C. (2013) Thermodynamic basis for evolution of apatite in calcified tissues. The American Mineralogist, 98, 2037-2045.

Spear, F.S., and Pyle, J.M. (2002) Apatite, monazite, and xenotime in metamorphic rocks. In Phosphates: Geochemical, Geobiological, and Materials Importance, Kohn, M.J., Rakovan, J.F., and Hughes, J.M., Eds., Reviews in Mineralogy and Geochemistry, 48, 293-335.

Taitai, A., and Lacout, J.L. (1987) Hydroxylation and fluorination of europium containing oxyapatites. Journal of Physics and Chemistry of Solids, 48(7), 629-633.

Ternane, R., Trabelsi-Ayedi, M., Kbir-Ariguib, N., and Piriou, B. (1999) Luminescent properties of Eu^{3+} in calcium hydroxyapatite. Journal of Luminescence, 81(3), 165-170.

Trueman, C. N. ;Tuross, N. (2002) Trace elements in recent and fossil bone apatite. Phosphates: Geochemical, Geobiological, and Materials Importance, 48, 489-521.

Tutken, T. ,Vennemann, T. W. ,Pfretzschner, H. U. (2011) Nd and Sr isotope compositions in modern and fossil bones - Proxies for vertebrate provenance and taphonomy. Geochimica Et Cosmochimica Acta, 75(20), 5951-5970.

Ushakov, S.V., Helean, K.B., Navrotsky, A., and Boatner, L.A. (2001) Thermochemistry of rare-earth orthophosphates. Journal of Materials Research, 16(9), 2623-2633.

Vandecandelaere, N., Rey, C., and Drouet, C. (2012) Biomimetic apatite-based biomaterials: On the critical impact of synthesis and post-synthesis parameters. Journal of Materials Science: Materials in Medicine, 23(11), 2593-2606.

Verron, E., Khairoun, I., Guicheux, J., and Bouler, J.-M. (2010) Calcium phosphate biomaterials as bone drug delivery systems: A review. Drug Discovery Today, 15(13/14), 547-552.

Weber, C., Mueller, M., Vandecandelaere, N., Trick, I., Burger-Kentischer, A., Maucher, T., and Drouet, C. (2013) Enzyme-functionalized biomimetic apatites: Concept and perspectives in view of innovative medical approaches. Journal of Materials Science: Materials in Medicine, 1-12.

Yamashita, K., Owada, H., Nakagawa, H., Umegaki, T., and Kanazawa, T. (1986) Trivalent-cation-substituted calcium oxyhydroxyapatite. Journal of the American Ceramic Society, 69(8), 590-594.

Yang, P., Quan, Z., Li, C., Kang, X., Lian, H., and Lin, J. (2008) Bioactive, luminescent and mesoporous europium-doped hydroxyapatite as a drug carrier. Biomaterials, 29(32), 4341-4347.

Figure Captions

Figure 1. XRD patterns obtained for increasing Ln^{3+} content: typical case of the europium doping series, with indexation according to the JCPDS #09-432 card. Inset: zoom on (002) diffraction peak

Figure 2. FTIR spectra for increasing Ln^{3+} content: typical case of the europium doping series (0, 2 and 7 mol % Eu initial)

Figure 3. Enthalpies of formation $\Delta H°_{f,ox}$ of Ln-doped apatites vs. Ln/(Ln+Ca) molar ratio. The undoped sample is shown on each graph in black. a) Eu -doped samples, b) Er-doped samples, c) Nd-doped samples, and d) Tb-doped samples

Figure 4. Difference between enthalpies of formation of doped and undoped samples vs. dopant radius for $Ca_{10-x-y}Ln_y(PO_4)_{6-x}(HPO_4)_x(OH)_{2-x-y}O_y{\cdot}nH_2O$ (Ln = Eu, Er, Nd, and Tb) for an experimental dopant content of y = 0.04

Tables

Table 1: Possible mechanisms for lanthanide (Ln^{3+}) doping in calcium phosphate hydroxyapatite (Al-Kattan et al., 2010a)

Mechanism 1:		
$3Ca^{2+} \rightarrow 2Ln^{3+} + \square_{Ca}$	$\rightarrow$	$Ca_{10-x-3y/2}Ln_y(\square_{Ca})_{x+y/2}(PO_4)_{6-x}(HPO_4)_x(OH)_{2-x}(\square_{OH})_x$ $(x\leq 2)$
Mechanism 2:		
$Ca^{2+} + HPO_4^{2-} \rightarrow 2Ln^{3+} + PO_4^{3-}$	$\rightarrow$	$Ca_{10-x-y}Ln_y(\square_{Ca})_x(PO_4)_{6-x+y}(HPO_4)_{x-y}(OH)_{2-x}(\square_{OH})_x$ $(x\leq 2;\ y\leq x)$
Mechanism 3:		
$Ca^{2+} + \square_{OH} \rightarrow Ln^{3+} + OH^-$	$\rightarrow$	$Ca_{10-x-y}Ln_y(\square_{Ca})_x(PO_4)_{6-x}(HPO_4)_x(OH)_{2-x+y}(\square_{OH})_{x-y}$ $(0\leq x-y\leq 2;\ y\leq x)$
Mechanism 4:		
$Ca^{2+} + OH^- \rightarrow Ln^{3+} + O^{2-}$	$\rightarrow$	$Ca_{10-x-y}Ln_y(\square_{Ca})_x(PO_4)_{6-x}(HPO_4)_x(OH)_{2-x-y}(O)_y(\square_{OH})_x$ $(x+y\leq 2)$

Table 2: Overall compositions of the precipitated samples, as determined from ICP, TG/DSC and XRD data. Mechanism 4 was applied, adapting the general formula: as $Ca_{10-x-y}Ln_y(PO_4)_{6-x}(HPO_4)_x(OH)_{2-x-y}O_y \cdot nH_2O$ and Ln = Eu, Er, Nd, and Tb ($0 \leq y \leq 0.10$)

Sample	Ca^{2+}	Ln^{3+}	PO_4^{3-}	HPO_4^{2-}	OH^-	O^{2-}	H_2O	$Ln(OH)_3$	$Ln^{3+}/(Ln^{3+}+Ca^{2+})$[8]
CaP	9.96	0.00	5.96	0.04	1.96	0.00	2.07	0.00	0.00
CaEuP1	9.62	0.18	5.79	0.21	1.62	0.18	2.16	0.00	0.02
CaEuP4	9.03	0.34	5.37	0.63	1.03	0.34	2.81	0.30	0.04
CaEuP7	8.36	0.55	4.91	1.09	0.36	0.55	4.52	0.55	0.06
CaEuP10	8.08	0.79	4.87	1.13	0.08	0.79	4.66	0.76	0.09
CaErP1	9.60	0.18	5.78	0.22	1.60	0.18	2.41	0.00	0.02
CaErP2	9.32	0.35	5.66	0.34	1.315	0.35	2.50	0.00	0.04
CaErP4	9.12	0.43	5.55	0.45	1.12	0.43	2.80	2.28	0.05
CaErP7	8.75	0.60	5.35	0.66	0.75	0.60	4.52	0.53	0.07
CaErP10	8.22	0.72	4.94	1.06	0.22	0.72	4.00	0.71	0.08
CaNdP1	9.52	0.19	5.71	0.29	1.52	0.19	1.86	0.00	0.02
CaNdP2	9.21	0.35	5.56	0.44	1.21	0.35	2.58	0.00	0.04
CaNdP7	8.54	0.46	5.00	1.00	0.54	0.46	4.40	0.55	0.05
CaNdP10	8.12	0.62	4.74	1.26	0.12	0.62	4.73	0.76	0.07
CaTbP2	9.24	0.36	5.60	0.40	1.24	0.36	2.77	0.00	0.04
CaTbP4	8.63	0.53	5.16	0.84	0.63	0.53	3.14	0.30	0.06
CaTbP7	8.55	0.90	5.45	0.55	0.55	0.90	4.39	0.57	0.09
CaTbP10	8.34	1.26	5.60	0.40	0.34	1.26	5.60	0.81	0.13

* Experimental $Ln^{3+}/(Ca^{2+}+Ln^{3+})$ molar ratio in the corresponding apatite phase

Table 3: Enthalpies of drop solution (ΔH_{ds}) of apatites, binary oxides, and lanthanide hydroxides in $3Na_2O{\cdot}4MoO_3$ at 973 K, and enthalpies of formation at 298 K of apatites from constituent oxides ($\Delta H^{\circ}_{f,ox}$) and from the elements taken in their standard state ($\Delta H^{\circ}_{f,el}$)

Binary compounds	ΔH_{ds} (kJ/mol)	Apatite samples	ΔH_{ds} (kJ/mol)	$\Delta H^{\circ}_{f,ox}$ (kJ/mol)	$\Delta H^{\circ}_{f,el}$ (kJ/mol)[d]
CaO	-90.70 ± 1.69[a]	CaP	1102.21 ± 8.94 (8)[b]	-2287.55 ± 9.65	-13307.5 ± 12.4
P_2O_5	-164.60 ± 0.85 [a]	CaEuP1	1078.75 ± 11.66 (14)	-2244.63 ± 12.50	-13173.1 ± 14.9
H_2O	69.00 ± 1.00[a]	CaEuP4	1149.31 ± 8.49 (10)	-2232.36 ± 9.43	-12894.1 ± 12.7
Eu_2O_3	-129.24 ± 2.12[a]	CaEuP7	1176.13 ± 10.75 (10)	-2101.71 ± 11.25	-12481.6 ± 14.3
Er_2O_3	-105.26 ± 2.48 [a]	CaEuP10	1194.01 ± 13.12 (12)	-2108.57 ± 14.02	-12474.7 ± 16.8
Nd_2O_3	-163.36 ± 3.44 [a]	CaErP1	1099.34 ± 12.02 (10)	-2247.75 ± 12.50	-13184.2 ± 14.7
Tb_2O_3	-125.58 ± 2.40 [a]	CaErP2	1109.33 ± 11.40 (11)	-2242.73 ± 7.01	-13139.1 ± 10.5
$Eu(OH)_3$	115.70 ± 1.27 (8)	CaErP4	1139.68 ± 11.42 (12)	-2205.22 ± 9.43	-13038.4 ± 12.2
$Eu(OH)_3$	117.73 ± 1.50[c]	CaErP7	1177.09 ± 15.77 (12)	-2146.12 ± 11.25	-12882.9 ± 13.7
$Er(OH)_3$	99.40 ± 1.80[c]	CaErP10	1154.85 ± 15.73 (12)	-2131.92 ± 14.02	-12627.4 ± 16.0
$Nd(OH)_3$	194.00 ± 2.40[c]	CaNdP1	957.55 ± 12.56 (9)	-2139.35 ± 12.56	-13024.5 ± 14.8
$Tb(OH)_3$	-41.50 ± 1.70[c]	CaNdP2	1025.24 ± 7.44 (8)	-2148.81 ± 7.44	-12958.9 ± 10.8
		CaNdP7	1021.77 ± 11.24 (10)	-1970.90 ± 11.24	-12439.3 ± 13.6
		CaNdP10	1089.21 ± 12.20 (8)	-1936.32 ± 12.20	-12259.8 ± 14.4
		CaTbP2	1041.67 ± 6.17 (8)	-2178.21 ± 7.01	-13025.3 ± 11.0
		CaTbP4	1070.18 ± 6.90 (8)	-2152.35 ± 9.43	-12746.4 ± 12.9
		CaTbP7	1145.46 ± 13.44 (10)	-2130.41 ± 11.25	-12965.9 ± 14.7
		CaTbP10	1205.79 ± 11.36 (8)	-2122.98 ± 14.02	-13109.5 ± 17.2

[a] From Ushakov et al. (Ushakov et al., 2001).
[b] Uncertainty is two standard deviations of the mean. The number in parentheses is the number of experiments.
[c] Calculated by considering the reaction $Ln(OH)_3 \rightarrow 1/2\ Ln_2O_3 + 3/2\ H_2O$ and the known values of ΔH°_f(hydroxide), ΔH°_f(oxide), ΔH_{ds}(oxide), ΔH_{hc}(H_2O gas, 298-973 K) and ΔH°_f(H_2O gas) (Robie et al., 1978).
[d] Calculated for the anhydrous apatite phases, considering the hydration water as thermodynamically equivalent to liquid water as was done previously

Table 4: Thermodynamic cycle for calculating the enthalpies of formation from the oxides of Ln-doped apatite samples based on mechanism 4, with Ln = Eu, Er, Nd, and Tb

Reaction[a]	ΔH
Ln_2O_3(s, 298 K) → Ln_2O_3(sol, 973 K)	$\Delta H_{ds}(Ln_2O_3)$
CaO(s, 298 K) → CaO (sol, 973 K)	ΔH_{ds}(CaO)
P_2O_5 (s, 298 K) → P_2O_5 (sol, 973 K)	$\Delta H_{ds}(P_2O_5)$[b]
H_2O (l, 298 K) → H_2O (g, 973 K)	$\Delta H_{ds}(H_2O)$[b]
$Ca_{10-x-y}Ln_y(PO_4)_{6-x}(HPO_4)_x(OH)_{2-x-y}\,O_y\,(H_2O)_n$ (s, 298K) → (10 – x – y) CaO (sol, 973K) + (y/2) Ln_2O_3 (sol, 973K)+ $3P_2O_5$ (sol, 973K) + (1 – y/2 + n) H_2O (g,973K)	ΔH_{ds}(Ln-apatite)
Formation reaction from the oxides: (10 – x – y) CaO (s, 298K) + (y/2) Ln_2O_3 (s, 298K)+ $3P_2O_5$ (s, 298K) + (1 – y/2 + n) H_2O (l,298K) → $Ca_{10-x-y}Ln_y(PO_4)_{6-x}(HPO_4)_x(OH)_{2-x-y}\,O_y\,(H_2O)_n$ (s, 298K)	$\Delta H^{\circ}_{f,ox}$**(Ln-apatite)**
Therefore $\Delta H^{\circ}_{f,ox}$**(Ln-apatite)** = (10 – x – y) ΔH_{ds}(CaO) + (y/2) $\Delta H_{ds}(Ln_2O_3)$ + $3\Delta H_{ds}(P_2O_5)$ + (1 – y/2 + n) $\Delta H_{ds}(H_2O)$	ΔH_{ds}(Ln-apatite)

[a]s = solid, l = liquid, g = gas, and sol = solution.
[b]Ushakov et al. (Ushakov et al., 2001).

Table 5: Evaluated thermodynamic properties of formation, from the elements (at 298 K), for the undoped and Ln-doped (Ln = Eu, Er, Nd, Tb) apatites prepared in this work

Apatite samples	$\Delta H^{\circ}_{f,el}$ (kJ/mol)	S° (J.mol^{-1}.K^{-1})	$\Delta S^{\circ}_{f,el}$ (J.mol^{-1}.K^{-1})	$\Delta G^{\circ}_{f,el}$ (kJ/mol)
CaP	-13307.5 ± 12.4	772 ± 9	-2682 ± 9	-12508.2 ± 13.4
CaEuP1	-13173.1 ± 14.9	768 ± 10	-2659 ± 10	-12380.7 ± 15.8
CaEuP4	-12894.1 ± 12.7	754 ± 10	-2607 ± 10	-12117.2 ± 13.8
CaEuP7	-12481.6 ± 14.3	739 ± 10	-2550 ± 10	-11721.7 ± 15.3
CaEuP10	-12474.7 ± 16.8	740 ± 10	-2536 ± 10	-11719.0 ± 17.8
CaErP1	-13184.2 ± 14.7	768 ± 9	-2654 ± 9	-12393.3 ± 15.6
CaErP2	-13139.1 ± 10.5	767 ± 9	-2634 ± 9	-12354.2 ± 11.7
CaErP4	-13038.4 ± 12.2	764 ± 9	-2617 ± 9	-12258.6 ± 13.3
CaErP7	-12882.9 ± 13.7	759 ± 9	-2592 ± 9	-12110.4 ± 14.6
CaErP10	-12627.4 ± 16.0	746 ± 9	-2538 ± 9	-11871.1 ± 16.8
CaNdP1	-13024.5 ± 14.8	766 ± 9	-2646 ± 10	-12236.0 ± 15.7
CaNdP2	-12958.9 ± 10.8	763 ± 10	-2621 ± 10	-12177.9 ± 12.0
CaNdP7	-12439.3 ± 13.6	744 ± 10	-2556 ± 10	-11677.6 ± 14.7
CaNdP10	-12259.8 ± 14.4	737 ± 10	-2519 ± 10	-11509.2 ± 15.5
CaTbP2	-13025.3 ± 11.0	765 ± 10	-2626 ± 10	-12242.7 ± 12.2
CaTbP4	-12746.4 ± 12.9	751 ± 10	-2570 ± 10	-11980.5 ± 13.9
CaTbP7	-12965.9 ± 14.7	769 ± 10	-2582 ± 10	-12196.5 ± 15.6
CaTbP10	-13109.5 ± 17.2	781 ± 10	-2580 ± 10	-12340.7 ± 18.1

Figures:

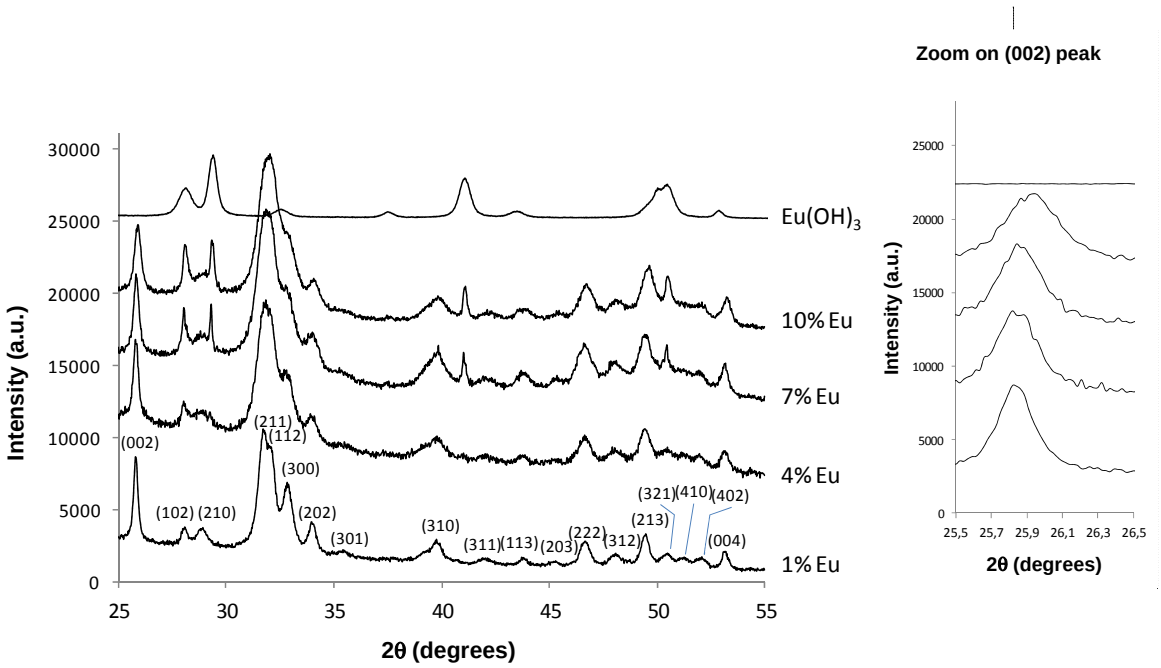

Figure 1

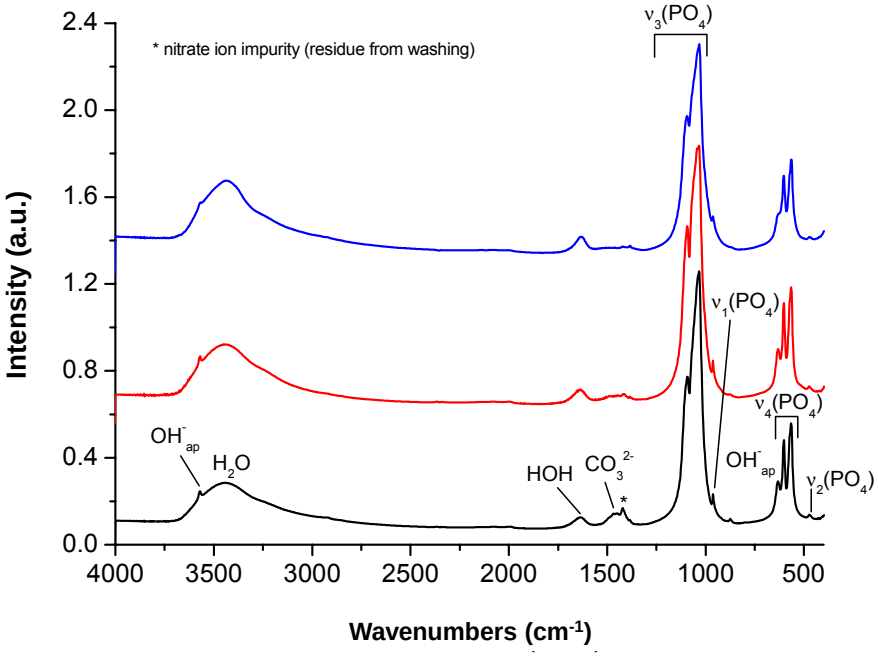

Figure 2

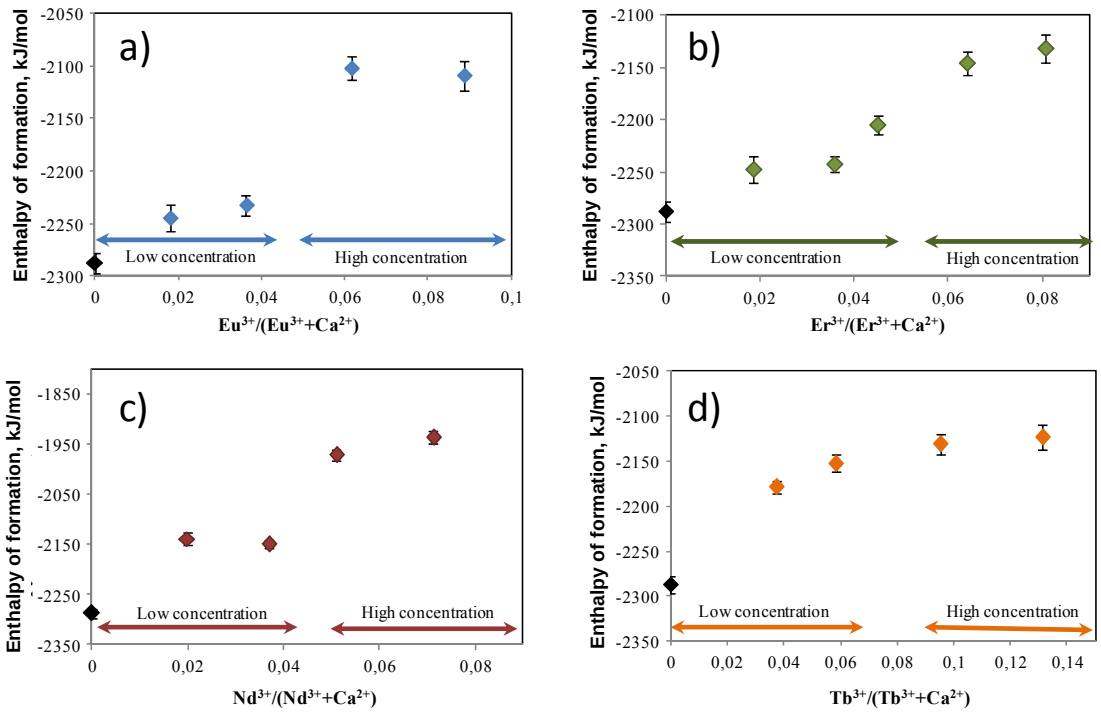

Figure 3

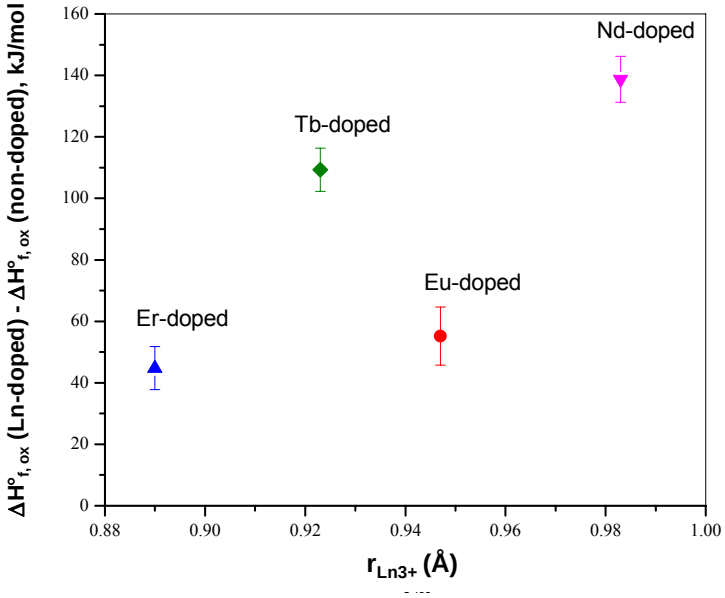

Figure 4